Supplement of The Cryosphere, 16, 1927–1940, 2022
https://doi.org/10.5194/tc-16-1927-2022-supplement

The Cryosphere
Open Access

Supplement of

Shear-margin melting causes stronger transient ice discharge than ice-stream melting in idealized simulations

Johannes Feldmann et al.

Correspondence to: Johannes Feldmann (johannes.feldmann@pik-potsdam.de)

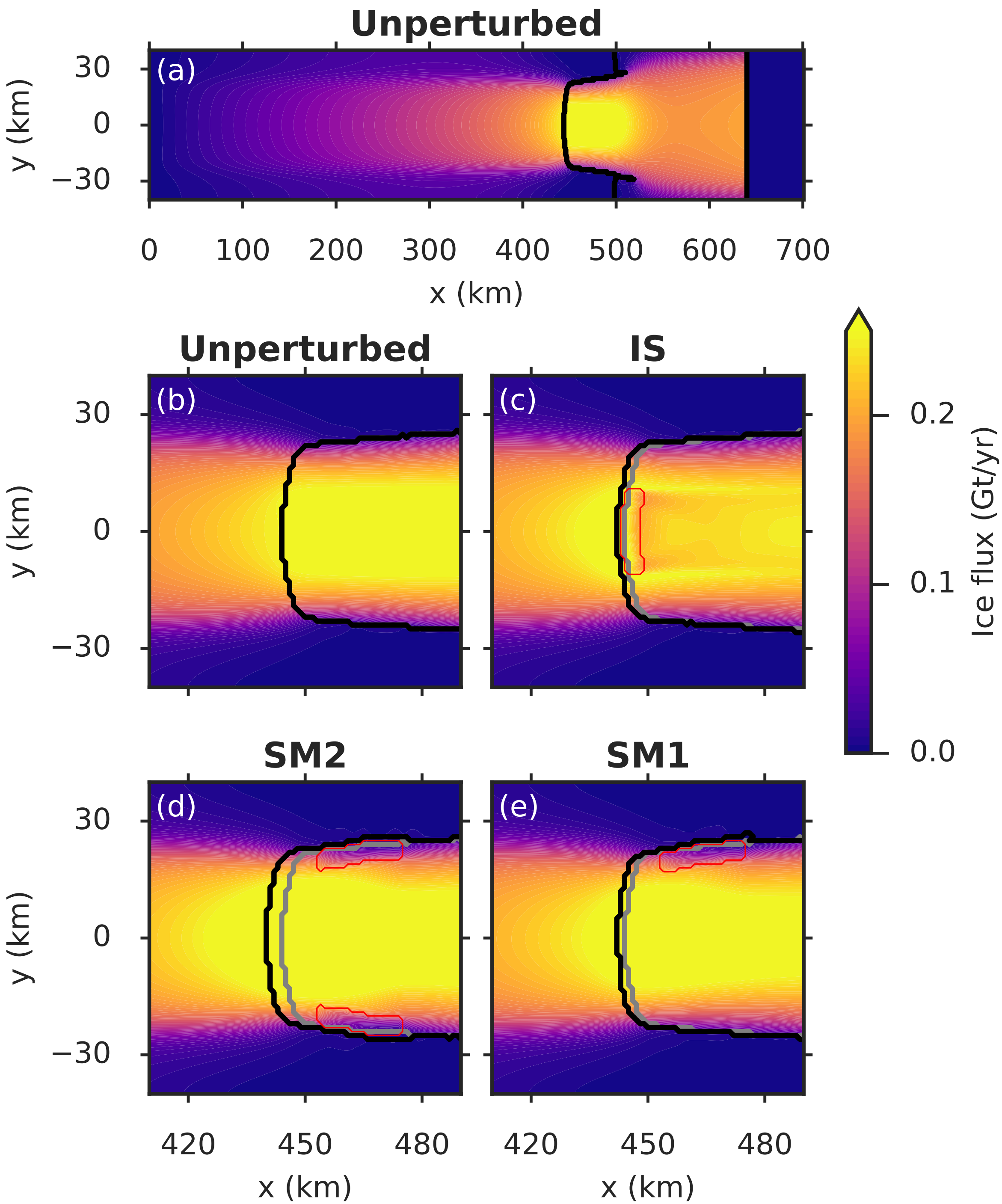

Figure S1. Comparison of the ice flux magnitude between **(a), (b)** the unperturbed steady state and **(c)-(e)** the perturbed states after 100 model years for each of the three melt experiments (see panel titles). The thin red contour denotes the perturbation area. Grounding line and calving front represented by black contours. Panels **(b)-(e)** show a zoom into the grounding-line region.

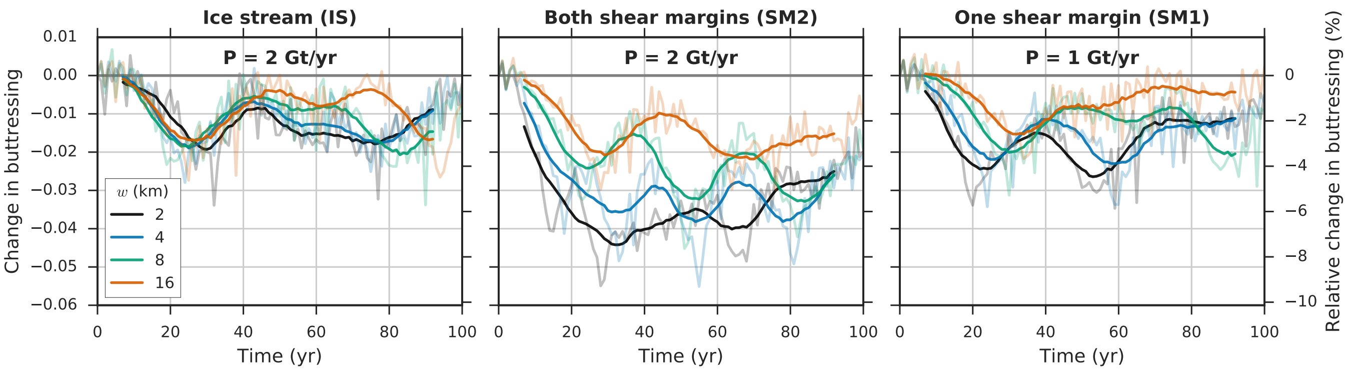

Figure S2. Time evolution of the buttressing number in response to the three perturbation types (columns) under a variation of the melt strip width (legend). The grounding-line retreat moderates the buttressing loss as the ice-shelf length increases (Dupont and Alley, 2005; Goldberg et al., 2009) and the perturbation area, tracking the grounding line, is shifted into a region of thicker ice. The buttressing number is diagnosed in flow direction (Fürst et al., 2016) in the center of the ice stream. In this specific case it is equivalent to the buttressing number from Gudmundsson et al. (2012) which is diagnosed in normal direction to the grounding line. The curves (legend) show the 15-year running mean of the yearly data (light colors). To reduce fluctuations the buttressing number is averaged over an area that spans the main part of the ice stream in y-direction (between $y = \pm 20$ km) and spans the sector between 10 and 20 km upstream of the grounding line in x-direction. Note that the total melt rate P is 2 Gt/yr in the IS and SM2 cases and 1 Gt/yr in the SM1 case for a better comparability between the SM1 and SM2 cases.

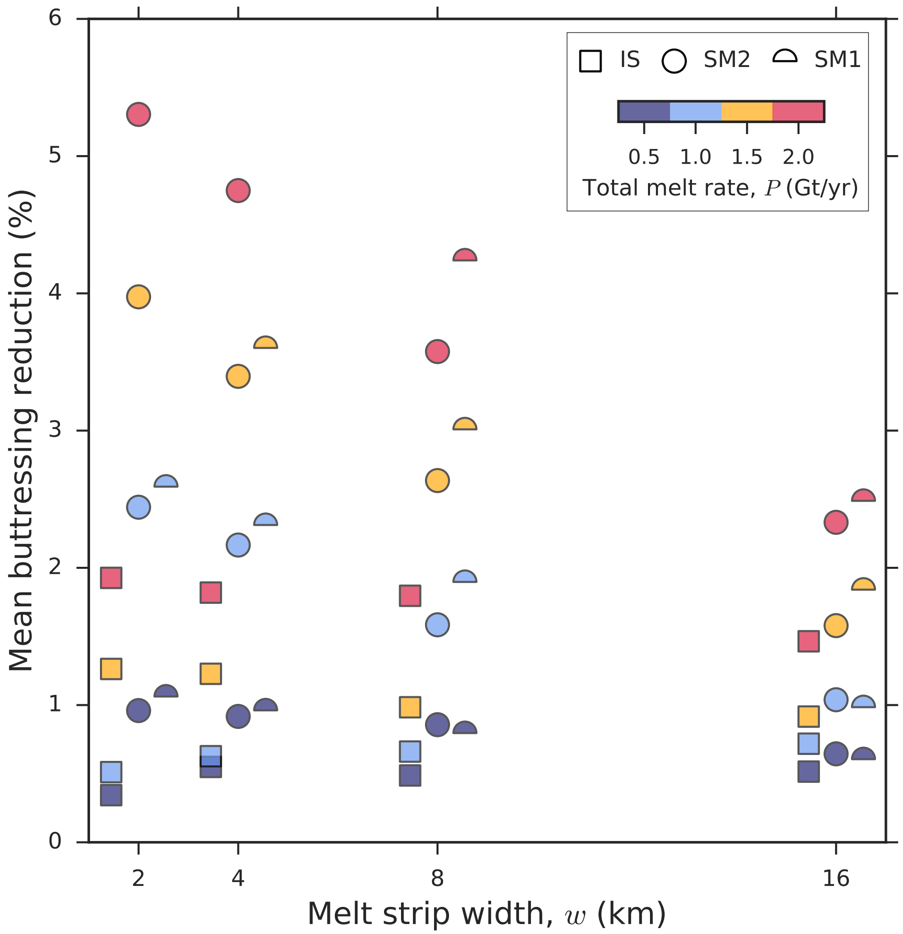

Figure S3. Time-averaged buttressing reduction dependent on the melt-strip width w (x-axis) and perturbation strength P (colorbar). The perturbation types are represented by individual symbols (legend). For better visibility the data points of the three perturbation types are slightly shifted against each other on the x-axis.

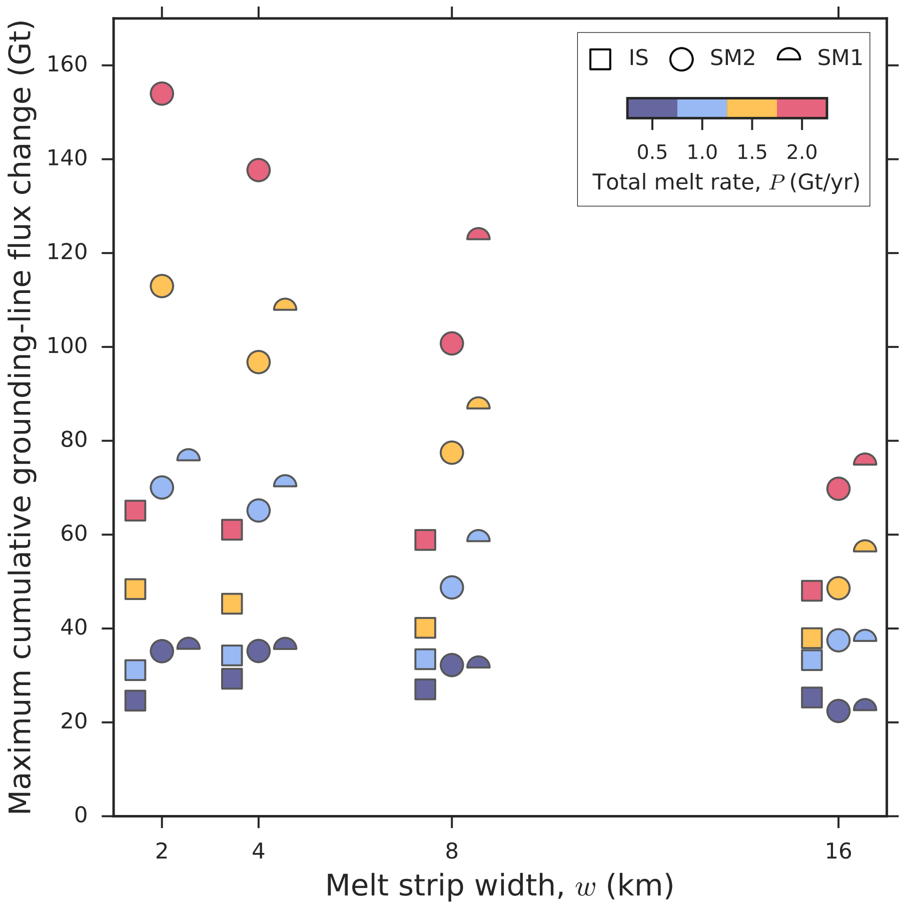

Figure S4. Maximum of the cumulative grounding-line-flux change dependent on the melt-strip width w (x-axis) and perturbation strength P (colorbar). The perturbation types are represented by individual symbols (legend). For better visibility the data points of the three perturbation types are slightly shifted against each other on the x-axis.

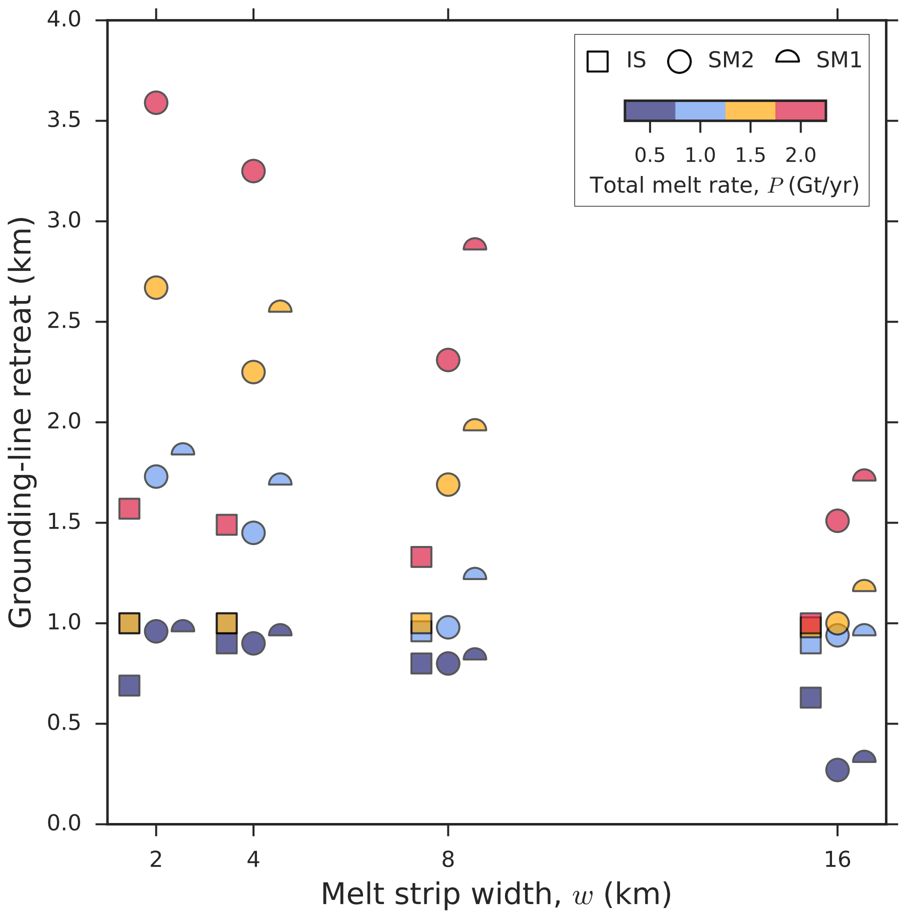

Figure S5. Centerline grounding-line retreat (average over the last 50 model years) dependent on the melt-strip width w (x-axis) and perturbation strength P (colorbar). The perturbation types are represented by individual symbols (legend). For better visibility the data points of the three perturbation types are slightly shifted against each other on the x-axis.

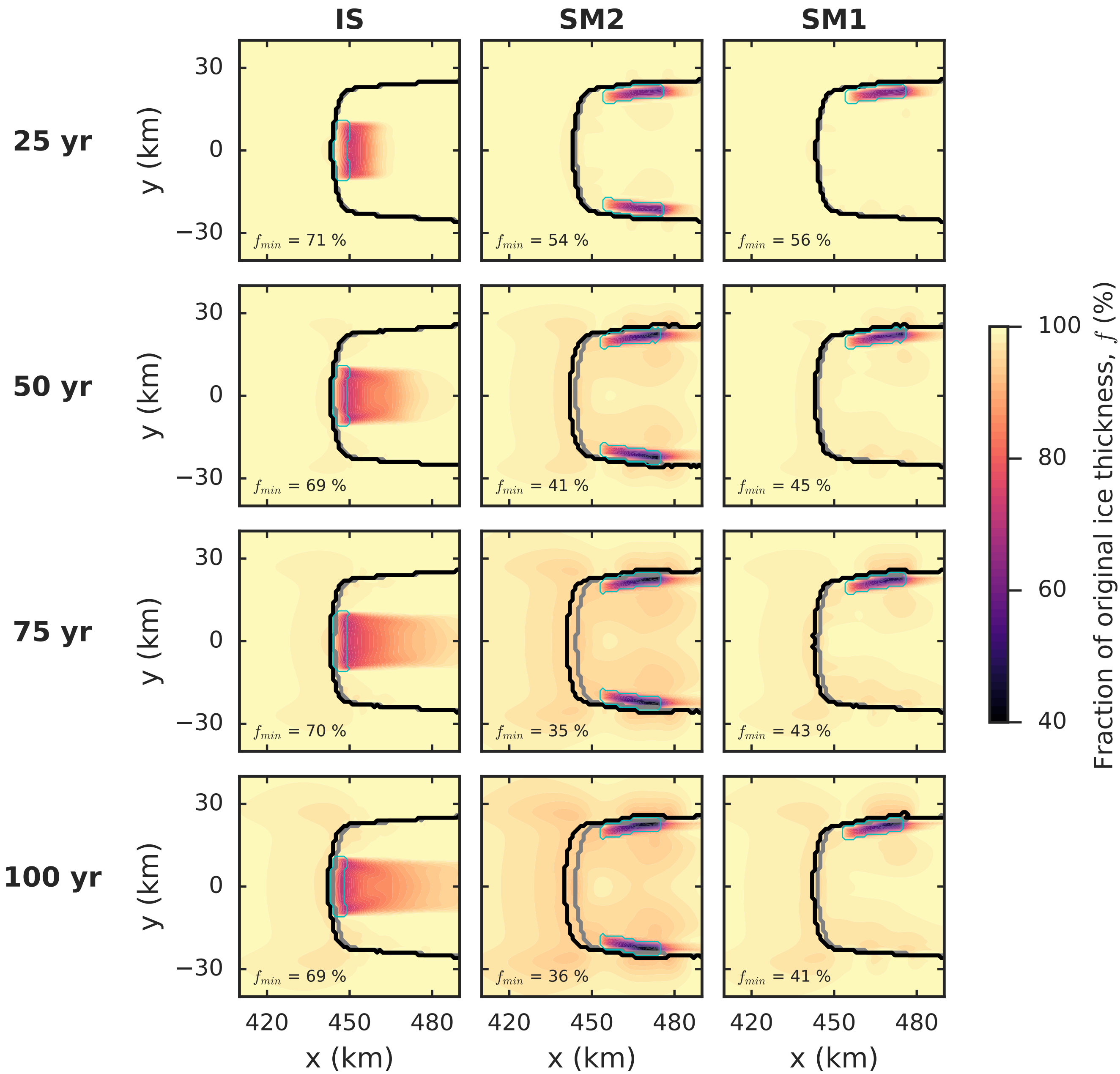

Figure S6. Fraction of initial ice thickness f (colorbar) in the vicinity of the grounding line at time slices of $25, 50, 75$ and 100 yr after the perturbation onset (rows) for the three different perturbation types (columns) and an applied melt-strip width of $w = 4$ km. In each panel the minimum value of f is given in the lower left corner. Thick contours represent the grounding-line position in the initial state (grey) and in the perturbed states (black). The thin cyan contour denotes the perturbation area. Note that the total melt rate P is 2 Gt/yr in the IS and SM2 cases and 1 Gt/yr in the SM1 case for a better comparability between the SM1 and SM2 cases.

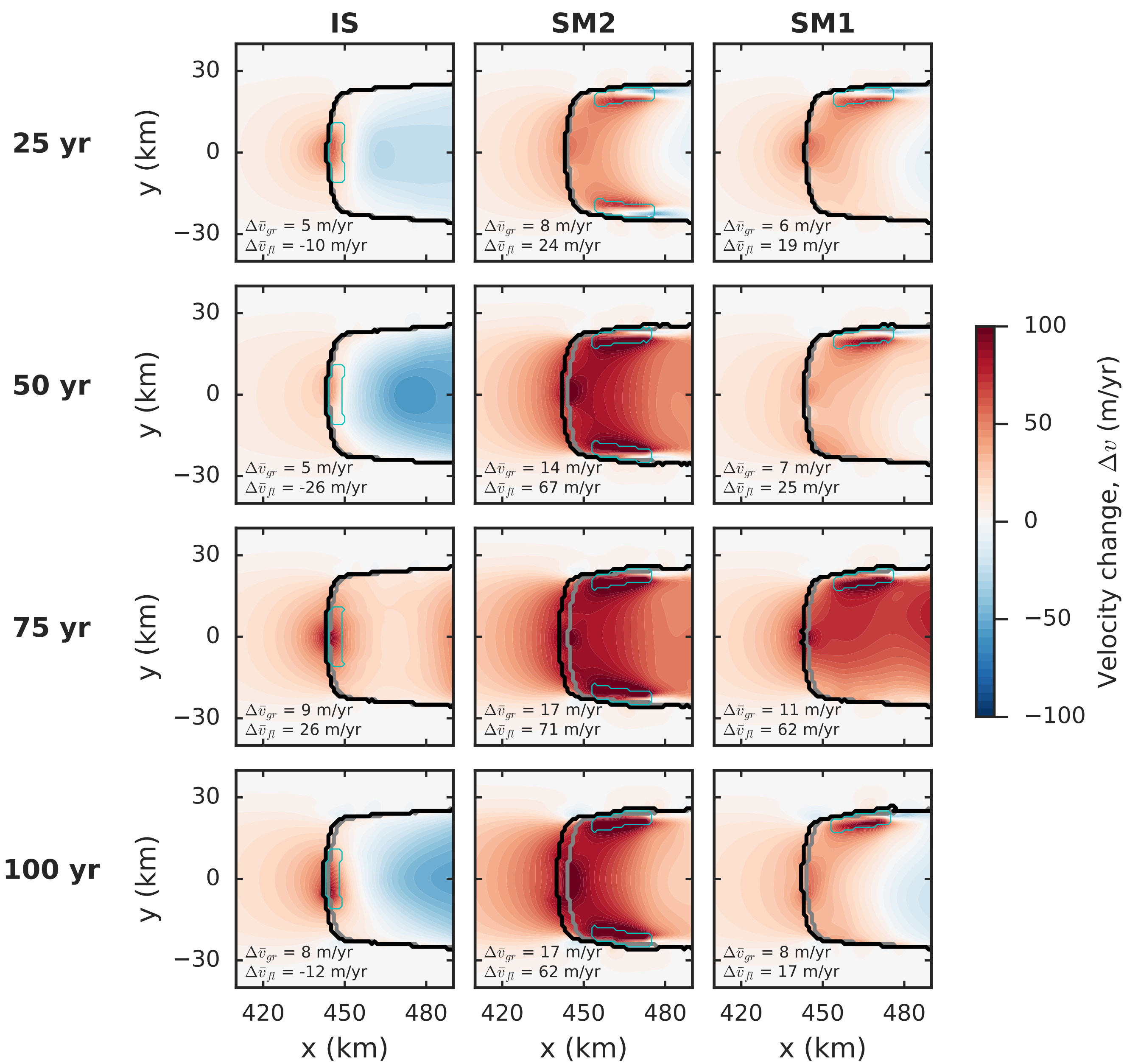

Figure S7. Change in ice speed Δv (colorbar) in the vicinity of the grounding line at time slices of $25, 50, 75$ and 100 yr after the perturbation onset (rows) for the three different perturbfation types (columns) and an applied melt-strip width of $w = 4$ km. In each panel the spatial mean of the grounded and floating speed changes (average over the displayed area), $\Delta\bar{v}_{gr}$ and $\Delta\bar{v}_{fl}$, respectively, are given in the lower left corner. Thick contours represent the grounding-line position in the initial state (grey) and in the perturbed states (black). The thin cyan contour denotes the perturbation area. Note that the total melt rate P is 2 Gt/yr in the IS and SM2 cases and 1 Gt/yr in the SM1 case for a better comparability between the SM1 and SM2 cases.

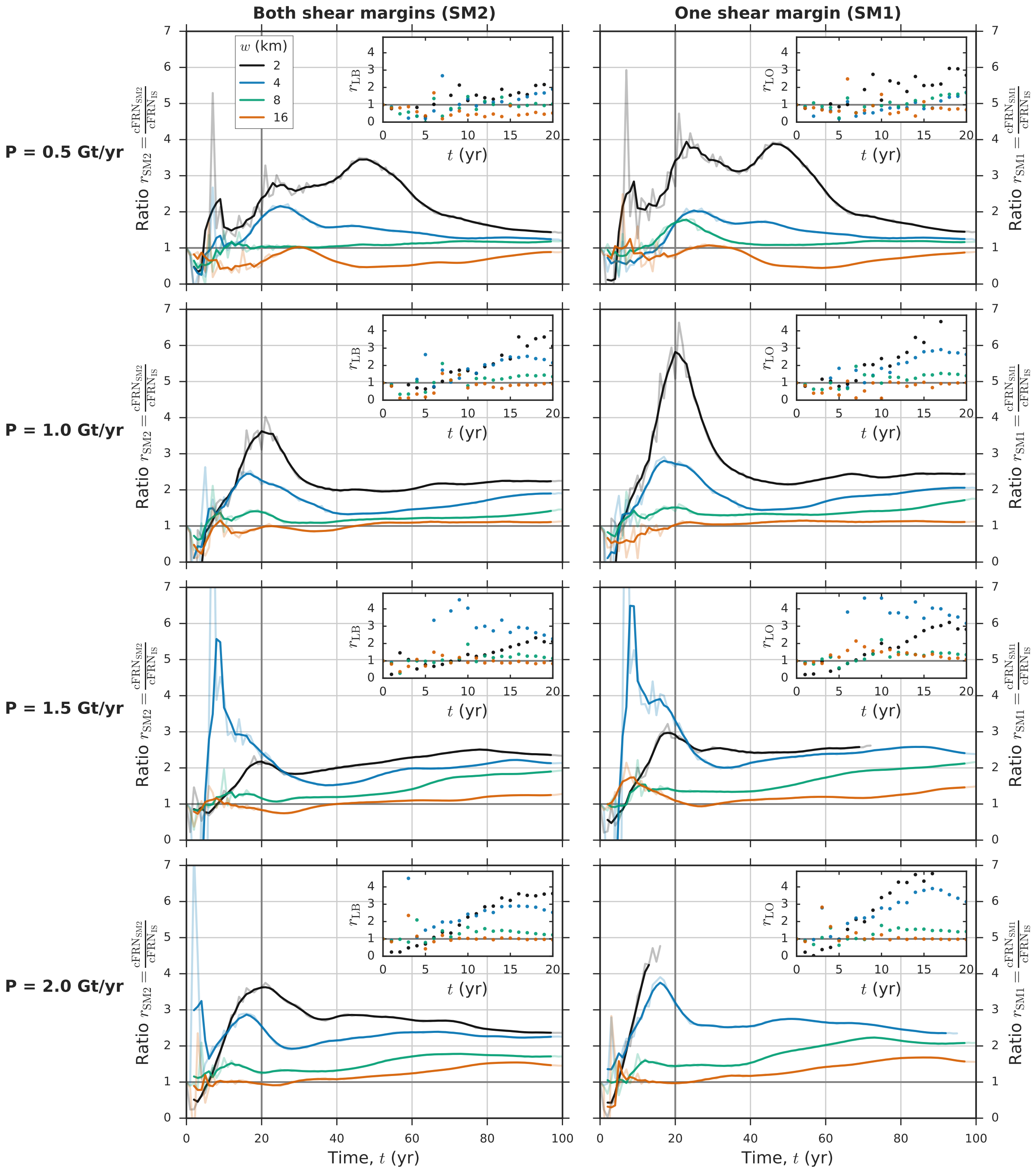

Figure S8. Time evolution of the cFRN ratios r_{SM2} and r_{SM1} for the two shear-margin perturbation experiments (columns), respectively, the four perturbation strengths P (rows) and the four melt strip widths w (colors given in the legend). The curves show the 5-year running mean of the yearly data (light colors). For each panel the yearly data points for the first 20 model years are shown in the corresponding inset.

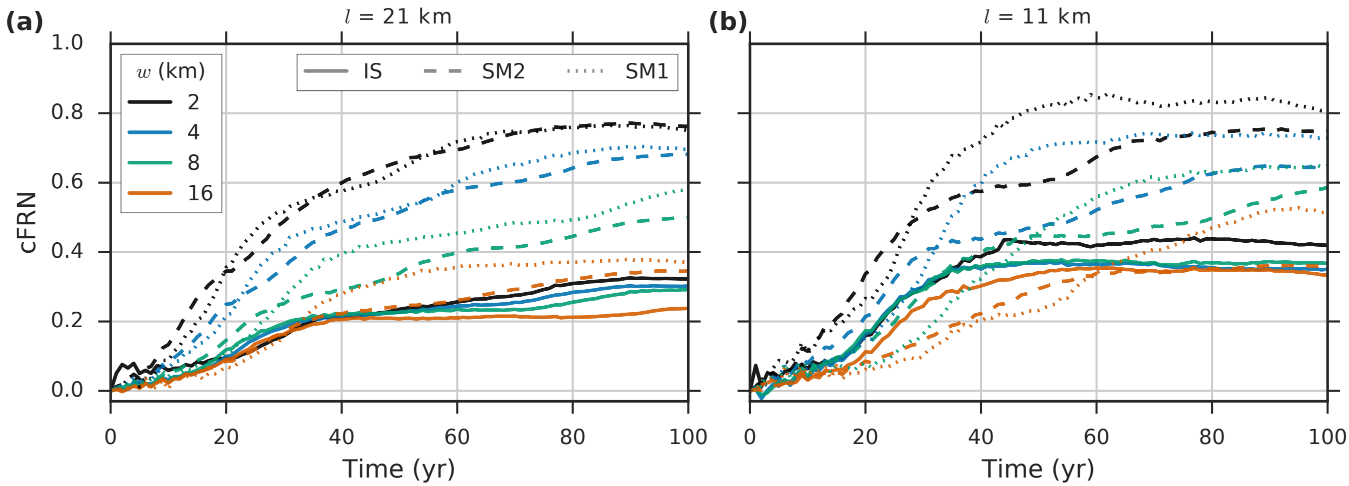

Figure S9. Comparison of cFRN curves (Eq. 1) between simulations using **(a)** the default melt-strip length $l = 21$ km (identical to Fig. 4) and **(b)** a reduced melt-strip length of $l = 11$ km. Each panel shows results for the three different perturbation experiments and the four applied melt-strip widths w (analogous to Fig. 4 of the manuscript). Note that in **(a)** the total melt rate P is 2 Gt/yr in the IS and SM2 cases and 1 Gt/yr in the SM1 case for a better comparability between the SM1 and SM2 cases. Since in **(b)** the melt areas are approximately halved, we also halved the total melt rates P in order to maintain similar local melt rates.

References

Dupont, T. K. and Alley, R. B.: Assessment of the importance of ice-shelf buttressing to ice-sheet flow, Geophysical Research Letters, 32, https://doi.org/10.1029/2004GL022024, https://agupubs.onlinelibrary.wiley.com/doi/abs/10.1029/2004GL022024, 2005.

Fürst, J. J., Durand, G., Gillet-Chaulet, F., Tavard, L., Rankl, M., Braun, M., and Gagliardini, O.: The safety band of Antarctic ice shelves, Nature Climate Change, 6, 479–482, https://doi.org/10.1038/nclimate2912, http://www.nature.com/articles/nclimate2912, 2016.

Goldberg, D., Holland, D. M., and Schoof, C.: Grounding line movement and ice shelf buttressing in marine ice sheets, Journal of Geophysical Research, 114, https://doi.org/10.1029/2008JF001227, http://doi.wiley.com/10.1029/2008JF001227, 2009.

Gudmundsson, G. H., Krug, J., Durand, G., Favier, L., and Gagliardini, O.: The stability of grounding lines on retrograde slopes, The Cryosphere, 6, 1497–1505, https://doi.org/10.5194/tc-6-1497-2012, https://www.the-cryosphere.net/6/1497/2012/, 2012.